Journal of The Electrochemical Society

The Electrochemical Society
Advancing solid state & electrochemical science & technology

OPEN ACCESS

Mapping Microscale Chemical Heterogeneity in Nafion Membranes with X-ray Photoelectron Spectroscopy

Mapping Microscale Chemical Heterogeneity in Nafion Membranes with X-ray Photoelectron Spectroscopy

Alicia K. Friedman,[=] Wenqing Shi,[=] Yaroslav Losovyj, Allen R. Siedle, and Lane A. Baker[*,z]

Department of Chemistry, Indiana University, Bloomington, Indiana 47405, USA

Nafion has found utility in a wide variety of applications, particularly as the most commonly used electrolyte membrane in fuel cell technology. Despite decades of characterization by X-ray Photoelectron Spectroscopy (XPS), a dispute exists within literature over the proper assignment of oxygen binding energies from the ether and sulfonate functional groups present in Nafion. Here, we have employed highly oriented pyrolytic graphite (HOPG) as an internal standard to calibrate all XPS spectra and are able to correlate binding energies from C1s, O1s, F1s and S2p to the Nafion structure. Further, microscale heterogeneities inherent to this formulation of Nafion membranes are revealed through two-dimensional XPS mapping of membrane cross-sections as well as surface ablation via Ar^+ ion sputtering. Results clearly show Nafion membranes are comprised of two chemically distinct layers: a surface layer several microns thick that is comprised of sulfonate groups and an inner layer that shields the more non-polar perfluoroether moieties.
 [DOI: 10.1149/2.0771811jes]

Manuscript submitted May 29, 2018; revised manuscript received August 13, 2018. Published August 28, 2018.

Membranes are critical components for controlling chemical, ion and electron flow in a number of important technologies. For example, polymer electrolyte membranes (PEMs) serve as all-in-one ion conductors, chemical barriers and mechanical supports for fuel cells.[1] The high proton conductivity and chemical stability of persulfonic acid-based polymers, such as Nafion, have set the standard in realistic applications of modern PEMs.[2–5] In light of the numerous applications and fields that utilize this polymer, a better understanding of both the chemical and structural relationships of Nafion membranes promises to aid optimization of membrane performance and to improve future technologies.

The chemical structure of Nafion, consisting of a polytetrafluoroethylene (PTFE) backbone and fluorous-ether side chains that contain sulfonic acid head groups, is illustrated in Figure 1a.[2] The PTFE backbone gives Nafion good mechanical stability and chemical resistance. In membranes, the sulfonic acid head groups of Nafion segregate to form channels capable of selective proton conduction. Significant effort has been directed toward understanding the nanoscale composition and structure of Nafion.[2,6,7] Conductive channels, randomly packed in a parallel fashion and estimated to be between 1 to 3.5 nm in diameter,[6–8] have been found responsible for chemical selectivity. Previous studies have also shown that different methods in preparation of freestanding Nafion films result in differences in film morphology.[2,9] In typical fuel cell applications, Nafion membranes are pretreated prior to use with successive incubations in water, hydrogen peroxide solution and sulfuric acid solution at elevated temperatures (outlined in Figure 1b).[10–16] This pretreatment process causes maximum swelling from water uptake in the membrane to create optimal conductivity for fuel cell applications. Hydrogen peroxide is thought to remove any organic contamination present, and this immersion step results in a visible color change of the membrane from slightly yellow to clear.[10,15,16] Exposure to sulfuric acid both removes any metallic impurities and introduces protons into the membrane that will eventually participate in the reduction half-reaction at the cathode of the fuel cell.[10,15,17]

Recently, we have examined effects of chemical degradation via Fenton chemistry on the ion-transport properties of Nafion membranes. In our initial report, we were primarily concerned with electrochemical characterization of membrane transport properties via scanning electron microscopy (SEM) and scanned probe microscopy.[18] Now, we have also employed X-ray photoelectron spectroscopy (XPS) and XPS elemental and oxidation state mapping to study the specific chemistry of these heterogeneous surface structures. A representative micrograph of a degraded Nafion membrane is shown in Figure 1c after accelerated breakdown upon exposure to Fenton's reagent for 12 h. Defects in the form of micro/nanoscale bubbles/tears are observed throughout the exposed surface. This heterogeneous topography can be attributed to chemical oxidation and change in membrane composition (which ultimately leads to altered membrane transport properties). Defects at the Nafion surface also exhibit chemical heterogeneity, as visualized in the false-color XPS map of oxygen in Figure 1d. Here, a degraded membrane was analyzed via XPS and the peak intensitiy of two different O1s binding energies mapped (533.1 eV in red, 535.5 eV in blue). As one signal is primarily localized over bubble defects and the other signal can be observed over the unmodified and intact membrane, an overall heterogeneous distribution of chemical composition is found at the membrane surface.

XPS has been employed frequently for study of PFSA polymer membranes to quantitatively determine the elemental composition, oxidation state and functional groups present. Additionally, XPS has served as a routine tool to confirm chemical modification of Nafion and other polyelectrolyte membranes, where introduction of various catalyst coatings and/or nanoparticles has demonstrated improved transport properties.[19–21] Our initial study revealed two especially important aspects related to the characterization and structure of a popular commercial version of Nafion film that are described in further detail here. First, XPS analyses of Nafion materials in literature are largely inconsistent in terms of spectral assignment and chemistry. In this report, by utilizing an internal standard of highly oriented pyrolytic graphene (HOPG) to correct binding energy shifts, we resolve peak assignments for carbon, oxygen, sulfur and fluorine. Second, with elemental oxidation state mapping studies of membrane cross-sections and sputtering experiments on membrane surfaces, we highlight inherent microscale heterogeneities through the thickness of the membrane that are present in untreated and exacerbated in treated Nafion films. To our knowledge, this heterogeneity on the microscale has not been previously discussed in XPS studies and may prove especially important for applications of commercial films and for future characterization and efforts to optimize or expand applications of Nafion membranes.

Experimental

Chemicals and materials.—Chemicals were used as received without further purification. Deionized water was purified with a Milli-Q system to an ultra-pure conductivity of 18 MΩ·cm (Millipore Corp., Danvers, MA). Nafion membranes were purchased from FuelCellsEtc (College Station, TX) and cut into smaller samples of dimensions ~ 1 × 1 cm. Sulfuric acid (Sigma Life Science, St. Louis, MO) and 30%

[=]These authors contributed equally to this work.
[*]Electrochemical Society Member.
[z]E-mail: lanbaker@indiana.edu

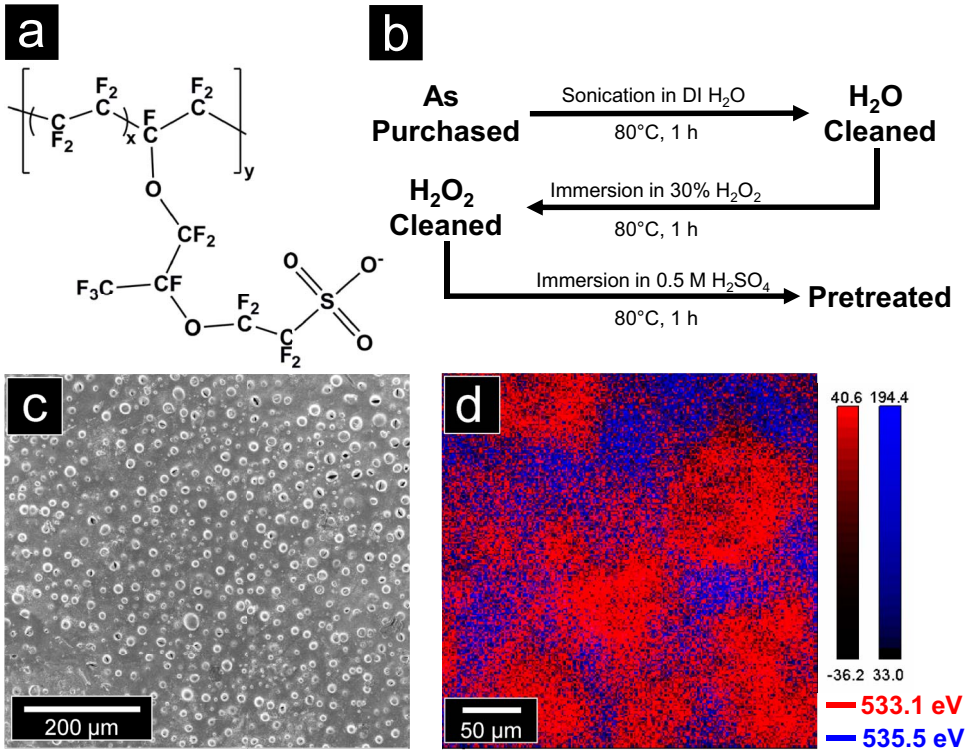

Figure 1. Chemical structure of Nafion (a) and the pretreatment protocol steps applied to membranes in preparation for use in fuel cells. Surface defects are observed in the scanning electron micrograph of a Nafion 212 membrane after incubation with Fenton's reagent for 12 h (c). A 2-D X-ray photoelectron spectroscopy (XPS) map highlights the heterogeneous surface chemistry of degraded Nafion (d). Here, two O1s peak binding energy signals are overlaid – 533.1 eV (sulfonate oxygens) in red and 535.5 eV (ether oxygens) in blue.

hydrogen peroxide solution (Macron Chemicals, Phillipsburg, NJ) were used for membrane pretreatment. Ferrous sulfate heptahydrate (Sigma Life Science) was used to accelerate membrane degradation and initiate surface imperfections on Nafion membranes. Highly oriented pyrolytic graphite (HOPG, grade ZYB) was purchased from Advanced Ceramics Inc. (Cleveland, OH).

Nafion membranes.—Two types of Nafion membranes (117 and 212) were used in these experiments. Though these membranes are identical in polymeric formulation with an equivalent weight of 1100 g/mol SO_3^- ($C_{20}F_{39}O_5S$, x = 6, y = 1), their cross-sectional thicknesses differ; Nafion 212, with a membrane thickness of 51 µm, is thinner relative to the 183 µm width of Nafion 117. Another difference in these formulations is the manufacturing method used for membrane preparation – Nafion 117 membranes are fabricated via polymeric extrusion whereas Nafion 212 membranes are solution cast to achieve a thinner membrane.

Nafion membrane pretreatment and degradation protocols.—A subset of Nafion membrane samples did not undergo the pretreatment process but rather were analyzed directly as received from the manufacturer (such samples are denoted as "As Purchased"). For Nafion membranes that were pretreated, a standard protocol was used as described previously,[12,14–16,18] with analysis performed after completion of different steps in the pretreatment process. Briefly, samples first were sonicated in DI water at 80°C for 1 h (denoted as "H_2O Cleaned"). Membranes then were immersed in 30% H_2O_2 at 80°C for 1 h to remove any organic impurities and rinsed off thoroughly with DI water (denoted as "H_2O_2 Cleaned"). Finally, samples were immersed in a solution of 0.5 M H_2SO_4 at 80°C for 1 h and rinsed repeatedly with DI water (denoted as "Pretreated"). Samples were stored in DI water at room temperature pending XPS analysis.

For cross-sectional analyses of Nafion, membranes were soaked in DI water for at least 24 h before dipped into liquid nitrogen until rigid and breakable. Forceps then were used to snap the membrane into two pieces and the membrane placed broken-edge-up on the platen for analysis. Use of a stereoscope aided in sample placement geometry, and care was taken to not touch or disturb the broken face of the membrane during this process. To minimize possible microstructure changes in the sample from exposure to air, the platen was placed immediately in the ultra-high vacuum environment of the XPS for analysis.

Nafion membrane degradation was achieved with Fenton's reagent in a protocol that has been described previously.[16,18] Briefly, wet Nafion membranes were incubated in 0.1 M $FeSO_4$ at 70°C for 2 h followed by copious rinses with DI water. The membranes then were incubated in 30% H_2O_2 at 70°C for 12 h and rinsed again with DI water. Finally, membranes were soaked in a solution of 0.5 M H_2SO_4 at 70°C for 2 h to remove any remaining iron.

SEM analysis.—Scanning electron microscopy (SEM) analysis was performed with an FEI Quanta 600 instrument (FEI, Hillsboro, OR) at 2.0 kV in secondary electron mode. Membranes were imaged with no additional sample preparation.

XPS analysis.—X-ray photoelectron spectroscopy (XPS) measurements were performed with a PHI *VersaProbe* II scanning X-ray microprobe with a focused Al K_α X-ray source (1486.6 eV) under ultra-high vacuum conditions (Physical Electronics (PHI), Chanhassen, MN). The X-ray beam was incident normal to the sample, and emitted photoelectrons were collected at an emission angle of 45° to the direction of incident X-ray. PHI dual charge compensation system was applied to all samples. Multiple samples for each experimental condition were analyzed, with all results consistent with the representative spectra presented here. Spectra were collected with

SMARTSoft-VP v.2.3.1 (PHI). Peak deconvolution and fitting were carried out with MultiPak v.9.3.0.3 (PHI) and/or CasaXPS (Casa Software Ltd., Teighnmouth, Devon, UK) software. High resolution scans were obtained with beam size of 200 μm and power setting of 49.5 W. Spectra were obtained with pass energies of 11.75 eV for C1s, 23.50 eV for O1s, 5.85 eV for F1s and 93.90 eV for S2p. Each data point (step size = 0.10 eV) was integrated over 2.16 sec, 2.4 sec, 2.0 sec and 0.96 sec for C1s, O1s, F1s and S2p, respectively.

For two-dimensional mapping experiments, a beam size of 9.0 μm, power of 0.9 W and pass energy of 117.40 eV was used with image dimensions of 100 × 100 pixels. Each data point (step size = 0.13 eV) was integrated over 0.015 sec, 0.025 sec, 0.01 sec and 0.075 sec for C1s, O1s, F1s and S2p, respectively.

For depth-profiling experiments, an Ar^+ ion gun operated at 0.5 kV was used to sputter away the membrane surface in 30 sec intervals; here, a beam size of 50 μm and power of 46.4 W was used. Pass energies of 23.50 eV for C1s, 46.95 eV for O1s, 23.50 eV for F1s and 93.90 eV for S2p were applied. Each data point (step size = 0.20 eV) was integrated over 0.24 sec, 0.56 sec, 0.24 sec and 0.80 sec for C1s, O1s, F1s and S2p, respectively.

A HOPG sample, attained via the "scotch-tape method,"[22] was used as an internal standard for binding energy correction. Simultaneous C1s spectra of both HOPG and an "As Purchased" Nafion sample were collected, and the C1s peak present in the HOPG spectrum manually assigned to the known sp^2 carbon binding energy of 284.4 eV. The corrected binding energy scale was subsequently applied to the Nafion spectrum. All sample spectra presented here were binding energy shifted to match the peaks from this calibrated sample.

Results and Discussion

Context of studies described.—Typical XPS studies of Nafion focus on C1s, O1s, F1s and S2p spectra. A definitive report focused on analysis of carbon-containing species in Nafion by XPS was detailed by Hoffman and coworkers[23] and provides an excellent benchmark for studies here. A binding energy E_b = 292.2 eV is expected for carbon in the $–CF_2–$ configuration, and signal at 284.8 eV in the C1s spectrum has been attributed to carbon in a graphitic state.[24,25] For the corresponding fluorine atoms, a binding energy of 689 eV is typically observed in perfluoropolyether polymers.[11,25–27] Sulfur of the sulfonic acid head group is assigned an E_b of ∼170 eV.[28,29] Oxygen is present in two different configurations within the chemical structure of Nafion. Oxygen is bound to sulfur within the sulfonic acid of the side chain ($–SO_3^-$) and also exists in ether groups of the side chains ($–F_2C–O–CF_2–$). These functional groups yield O1s signals at two distinct binding energies of 533.0 eV and 535.7 eV (ΔE_b of ∼2.7 eV). A close examination of XPS literature over the last few decades reveals discrepancies in assignment of these O1s peak signals to the two possible atomic configurations within the Nafion structure. Upon examination of 25 prior publications, 52% assign the peak at E_b ∼533.0 eV to oxygen atoms in the $–SO_3^-$ configuration and the peak at E_b ∼535.7 eV to oxygen in the ether configuration (n = 13 papers);[15,23,30–40] 40% assign the peaks in the opposite arrangement, with $–SO_3^-$ oxygen atoms identified as signal at 535.7 eV and ether atoms at 533.0 eV (n = 10).[41–50] Another two papers (8% of the literature) identify these binding energies as O1s signals but are careful not to differentiate or assign the peaks to specific configurations.[18,51] This inconsistency continues to plague even the most up-to-date literature, as multiple papers have been published in the last few years with opposing ether/sulfonic acid O1s peak assignments. (A complete listing of references, and respective O1s peak assignments in Nafion publications, is present in Table S1 of Supporting Information.)

With this work, we first seek to resolve inconsistencies found in literature and determine definitive O1s peak assignments from XPS analysis on Nafion membranes at different stages in the pretreatment process. Our data agree with previous studies to indicate the pretreatment process causes chemical changes within the membrane rather than simply cleaning the surface. In the course of this work, an organized microstructure with chemically different surface and bulk layers was also observed for Nafion membranes. The surface layer is present in both "As Purchased" and chemically treated membranes and extends several microns in thickness into the membrane, suggesting the chemical composition is truly heterogeneous at the microscale. The inner bulk layer, which we have observed both through depth profile analysis with Ar^+ ion sputtering and cross-sectional mapping of membranes, is found to be closer in chemical makeup as to what is expected from the molecular structure of the Nafion polymer.

XPS studies of pretreatment effects.—To analyze effects of pretreatment on the chemical composition of Nafion, high resolution XPS analysis was performed on the membranes at different stages during the process with sp^2 carbon signal from HOPG used to calibrate all binding energy measurements. Though many studies reference samples to a well-established peak assignment, even commonly referenced carbon peaks such as $–CF_2$ or $–CF_3$ can result in binding energy variation an order of magnitude greater than observed with HOPG calibration (∼0.5 eV vs. ∼0.05 eV, respectively).[52] For additional data on HOPG calibration, please refer to SI Figures S1 and S2. Representative C1s, O1s, F1s and S2p spectra are shown in Figure 2 for each pretreatment step with traces offset for easier visualization. From these spectra, overall elemental concentrations in atomic percentage were determined and are summarized in Table I, with theoretical values calculated for Nafion 212 (x = 6, y = 1, $C_{20}F_{39}O_5S$). For each step in the pretreatment protocol, the carbon, oxygen, fluorine and sulfur signals show the presence of peaks at comparable binding energies, meaning the type of functional groups and chemical environment for these groups present at the membrane surface remain unchanged. Binding energies for carbon are observed at ∼285.5 eV, 287.0 eV, 289.9 eV, 292.2 eV and 293. 6 eV (for deconvoluted and fitted C1s spectra, please refer to SI Figure S3). The primary peak observed at 292.2 eV corresponds to the carbon species present within the PTFE backbone ($–CF_2–CF_2–$). The shoulder at ∼293.6 eV is attributed to the $–CF_3$ functional group (in agreement with previous reports).[23] The peaks at ∼290 eV and ∼287 eV correspond to carbons in the $–OCF_2–$ and –CF– configurations, respectively. C1s signal present at ∼285.5 eV is most likely due to a surface layer of adventitious carbon present in nearly all samples analyzed via XPS. Both the F1s and S2p spectra show a single peak at ∼689.7 eV and ∼170.1 eV, respectively. Two binding energies are observed throughout these O1s spectra: a higher energy peak at 535.5 eV and a lower energy peak at 533.1 eV. The numerical values of binding energies measured are consistent with previous studies, but chemical assignment of the oxygen atoms to these peaks remains contentious in the literature. The higher binding energy peak (535.5 eV) correlates to oxygen present in the ether functional group and the lower binding energy signal (533.1 eV) to oxygen present in the sulfonate groups. These assignments can be explained by the respective partial atomic charges each type of oxygen atom experiences. Even though the oxygens in fluoroether functional groups are not directly bound to fluorine, the overall environment they experience is quite electronegative in comparison to the environment of the sulfonate oxygen atoms. As further evidence these are the proper O1s peak assignments, previous XPS studies of similar perfluoropolyether compounds assign the oxygen ($–CF_2–O–CF_2–$) to binding energies of ∼536 eV;[11,27,53] similarly, oxygens in sulfate and sulfonate functional groups are typically found at binding energies closer to ∼532 eV.[26,28,29] For studies in which O1s peaks were incorrectly assigned, authors likely did not consider the effect of neighboring fluoroalkanes on ether-bound oxygen atoms, as signal for a typical ether group is ∼533 eV.[54]

Though there is no change in which functional groups are present in Nafion, the relative abundance of these functional groups is altered during the pretreatment process. The most significant change in surface composition can be seen in the O1s spectra, which makes sense on a chemical level as solutions used in the pretreatment steps provide oxidizing environments. Figure 3 shows the O1s spectra in greater detail, including deconvolution and fits used to calculate the areas under each peak for quantification.

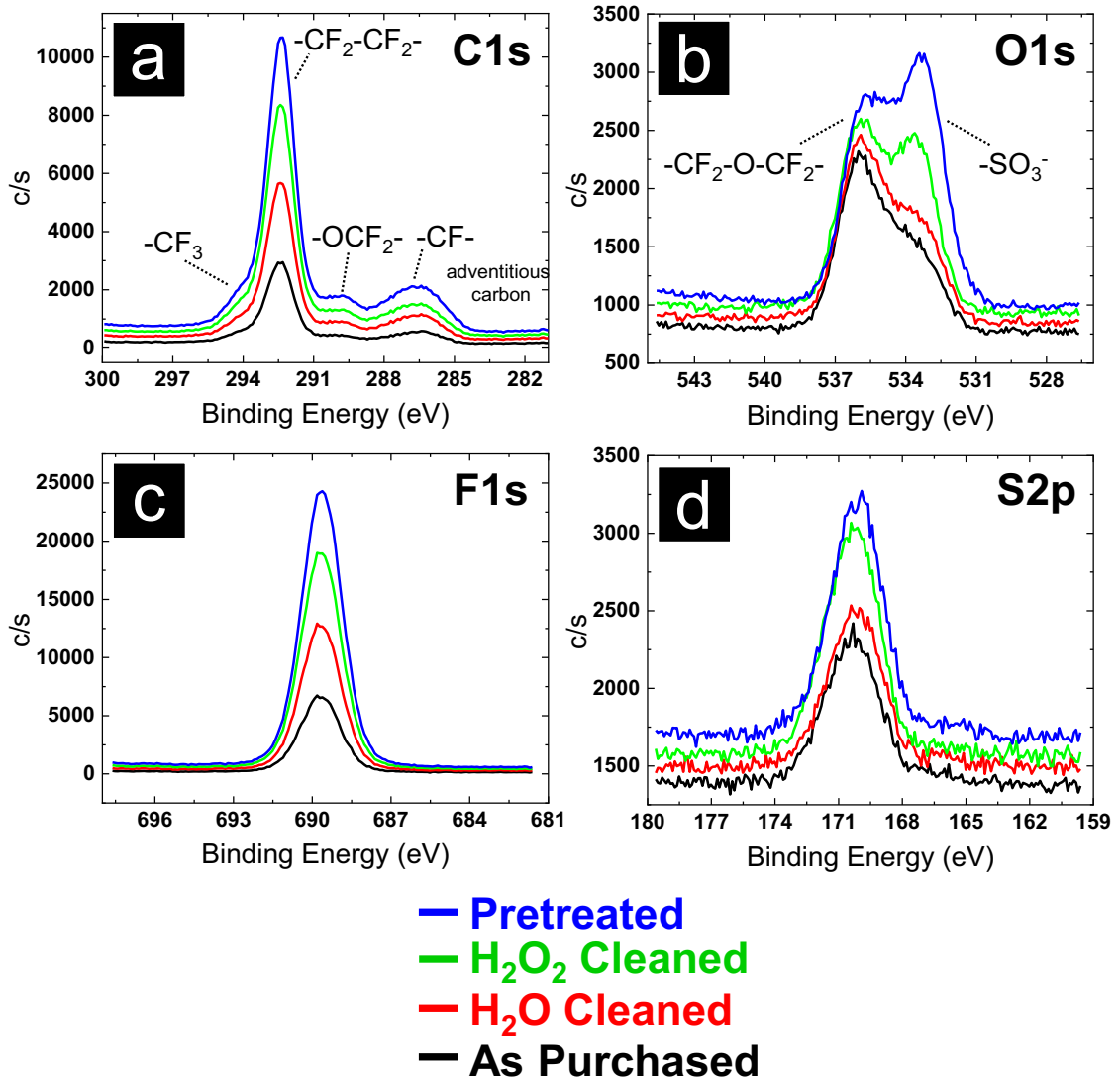

Figure 2. C1s (a), O1s (b), F1s (c) and S2p (d) spectra of Nafion membranes after each experimental step in the pretreatment process: "As Purchased" (black), "H_2O Cleaned" (red), "H_2O_2 Cleaned" (green), and "Pretreated" (blue). Traces have been offset for easier visualization.

Table I. Elemental composition (in atomic percentage) of Nafion membranes at different stages during the pretreatment process as determined from XPS spectra shown in Fig. 2.

Sample	C1s (%)	O1s (%)	F1s (%)	S2p (%)
Expected Values from Chemical Formula	30.8	7.7	60.0	1.5
As Purchased Membrane	*31.9*[a]	*7.0*	*60.3*	*1.0*
H_2O Cleaned Membrane	*31.6*	*7.3*	*60.3*	*0.9*
H_2O_2Cleaned Membrane	*31.5*	*7.8*	*59.6*	*1.2*
Pretreated Membrane	*30.4*	*10.6*	*57.8*	*1.4*

[a]Italicized entries are experimental results.

The initial immersion step in distilled water has little effect on the Nafion membrane, as comparable atomic percentages are observed for each element in the "As Purchased" and "H_2O Cleaned" membranes (Table I). Additionally, the O1s spectra collected for these two samples are nearly identical (Figures 3a and 3b, respectively), and a 3:2 ratio of ether oxygen atoms to sulfonate oxygens is observed at the surface of both membranes (~60% and 40% peak areas, respectively). After exposure to hydrogen peroxide solution, little change in carbon or fluorine surface concentration is observed for the "H_2O_2 Cleaned" sample. An increase in both sulfur and oxygen concentrations is noted, with a specific increase in sulfonate oxygen to ~ 46% of the total oxygen concentration (Figure 3c). Finally, after the sulfuric acid immersion step, a loss in both carbon and fluorine surface concentrations is observed in addition to an increase in oxygen and sulfur. In this "Pretreated" sample, a 2:3 ratio of ether oxygens to sulfonate oxygen atoms is measured (Figure 3d), a value that matches the chemical structure of the Nafion 212 membranes analyzed within these experiments. Note the intensity of the higher binding energy signal at 535.5 eV remains constant throughout the pretreatment process; changes in the O1s ratio are caused only by an increase in the sulfonate oxygen at the lower binding energy of 533.1 eV. The changes we observe during the pretreatment process in surface oxygen, sulfur and fluorine concentrations agree well with previously reported literature.[15]

Together, these data suggest the pretreatment procedure reorganizes the Nafion membrane for greater exposure of the sulfonate head groups at the surface. Reorganization such as that proposed here has also been postulated in previous studies by Schulze et al.,

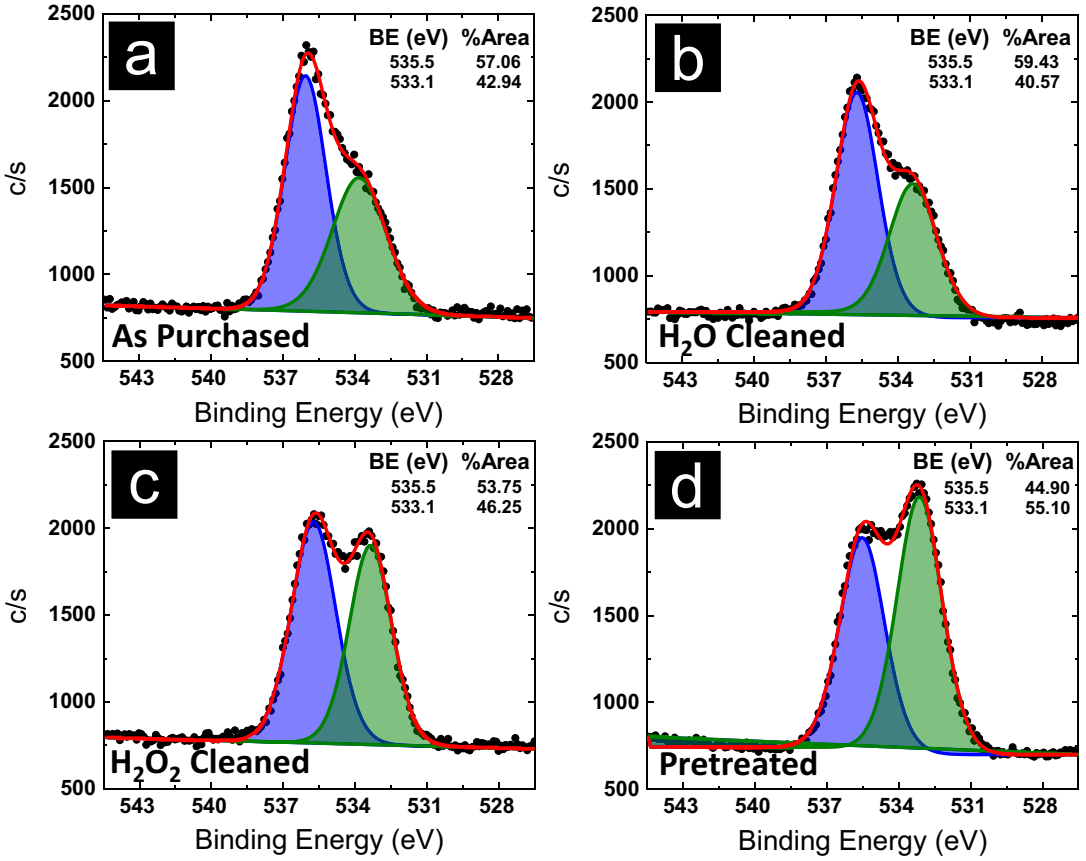

Figure 3. Deconvolution of O1s spectra for "As Purchased"(a), "H_2O Cleaned" (b), "H_2O_2 Cleaned" (c) and "Pretreated" Nafion membranes. Each overall modelled fit is plotted in red over actual data points (black), and individual curve fits are shown for 535.5 eV peaks in blue and 533.1 eV peaks in green. The calculated peak area percentages also are presented.

where changes observed were explained as a rotation of the polymer side chains to direct the sulfonic acid groups to the surface.[15] Results presented here agree with this study and support findings that pretreatment protocols trigger Nafion film reorganization to a predominance of sulfonate functional groups at the surface.

Chemical heterogeneity in Nafion.—The use of Fenton's reagent was found to induce microstructural defects in Nafion films that were manifested visually as bubbles, rips and tears (vide supra). Defects were found to possess different chemical compositions from XPS analysis, and we were extremely interested in understanding the origin/nature of these features. Close analysis at the surface of Nafion samples revealed random spatial areas with significantly different XPS signals, an indication of surface micro-heterogeneity. Figure 4 shows representative C1s and O1s spectra for both "As Purchased" and fully "Pretreated" membranes. Each graph shows three spectra collected from spatial points along the surface of a single membrane. Variation in the intensity of the binding energy peaks is present in both the carbon and oxygen analysis, which indicates changes in chemical composition. This heterogeneity is present in "As Purchased" membranes and remains even after the chemical pretreatment process. It is likely such heterogeneity arises from physical removal of the membrane surface due to defects such as scratches. These spatial areas, in which an inner layer of the membrane has been exposed, result in XPS spectra very different from the typical membrane surface results presented previously in Figure 2. In conjunction with the chemical heterogeneity observed over the degradation spots identified previously in Figure 1c, these data suggest the existence of a surface layer that is chemically unique from underlying bulk Nafion material.

To examine microstructural heterogeneities of Nafion films in more detail, two-dimensional XPS mapping was performed to visualize cross-sectional areas of membranes. Briefly, Nafion was flash frozen by immersion into liquid nitrogen and snapped in half, with the edge along the break analyzed with XPS mapping. This freeze-fracture method was employed over traditional cleavage methods (e.g. scissors, razors) to ensure the surface remained unmodified by the collection process itself, both due to transfer from a tool as well as microscopic changes in the integrity of the membrane.

Figure 5 shows C1s and O1s mapping results of spectra attained for the inner bulk (red) and outer surface (blue) layers of an "As Purchased" Nafion 212 membrane. Within the interior of the membrane (collected from the red box drawn in Figure 5a, mapped in Figure 5b and plotted in Figure 5e), $-CF_2-$ groups give the greatest C1s signal at 292.2 eV, with small contributions observed from adventitious carbon (~285 eV). The carbon composition of the surface layer (collected from the blue box drawn in Figure 5a, mapped in Figure 5c and plotted in Figure 5e, however, can mostly be attributed to a layer of adventitious carbon. When the corresponding surface (blue) and bulk (red) maps are overlaid (Figure 5d), the boundary that divides these two layers is discrete and sudden; the outer layer extends into the membrane interior several microns.

Even more striking is the difference between oxygen chemistry in these layers of the Nafion membrane. The chemical composition of the bulk layer (collected from the red box drawn in Figure 5f, mapped in Figure 5g and plotted in Figure 5j) is almost entirely dominated by oxygens from the sulfonate functional group (~533 eV). Within the inner portion of the membrane (collected from the blue box drawn in Figure 5f, mapped in Figure 5h and plotted in Figure 5j), the oxygens in the ether configuration are observed. Similar to the C1s analysis

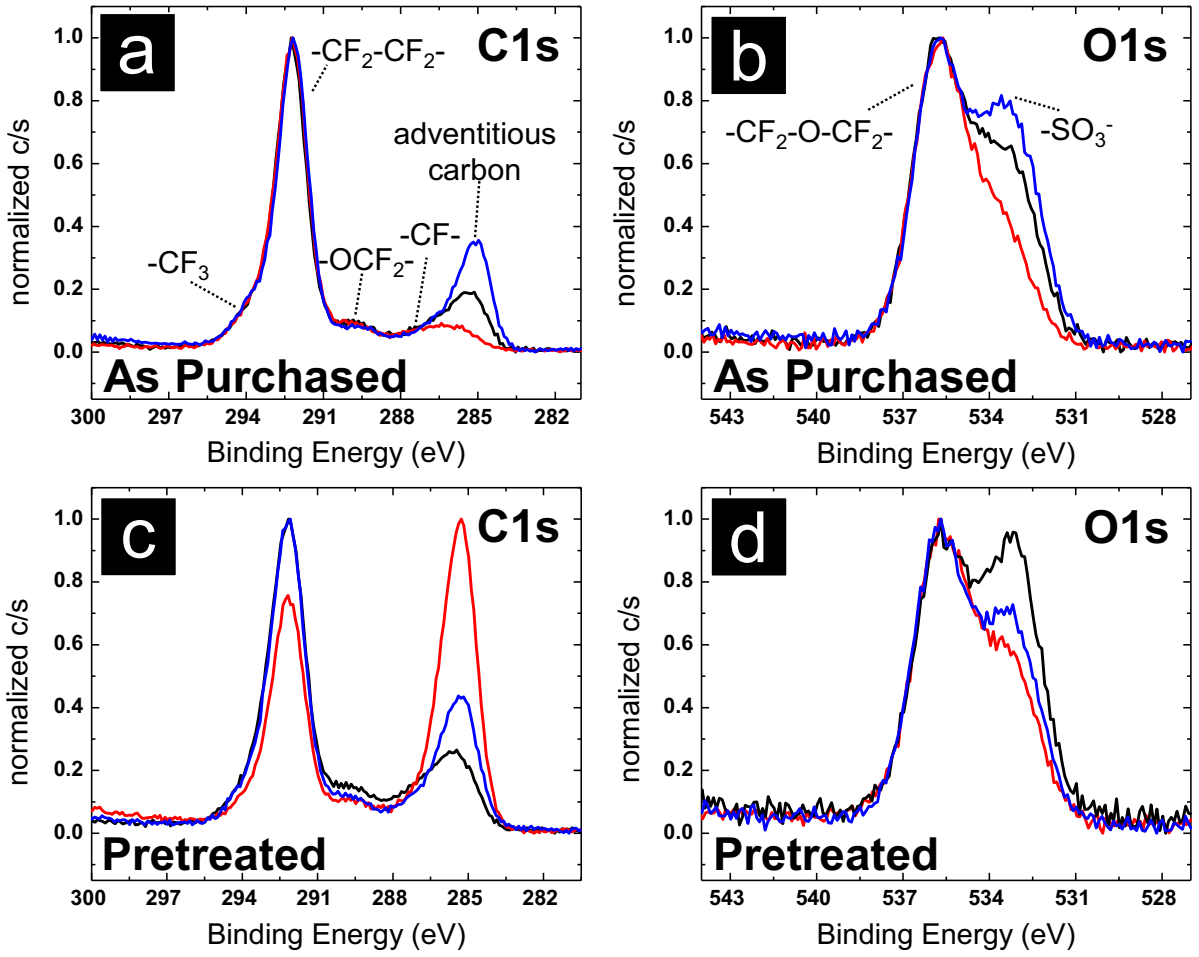

Figure 4. XPS spectra that highlight the chemical heterogeneity on the surface of Nafion membranes. C1s (a) and O1s (b) spectra measured for "As Purchased" membranes can be compared to C1s (c) and O1s (d) spectra of fully "Pretreated" membranes. Each trace (black, red and blue) represents analysis at a different spatial location of the membrane. Spectra have been normalized for easier visualization of differences in elemental composition.

above, overlaying the bulk and surface layer maps shows discrete heterogeneous layers (Figure 5i).

This layered chemical heterogeneity was observed in both Nafion formulations that were analyzed (212 and 117) and can be seen both before and after pretreatment has been performed (SI Figures S4, S5, S6). Additionally, the distance the surface layer extended into the membrane was similar for both formulations, but an extended length of inner bulk chemistry was observed for the thicker Nafion 117 film (SI Figure S7). These findings likely explain the occurrence of surface heterogeneity highlighted previously in Figure 4: microscopic scratches or surface defects have removed the outer surface layer to expose underlying bulk membrane. Additional evidence that membrane defects generate this chemically heterogeneous surface can be seen in SI Figure S8, in which spectra of a mechanically ablated membrane are similar in elemental composition to the inner bulk membrane.

The only previous mention of this unique microarchitecture within Nafion literature was reported by Xin and coworkers in 2004.[55] Briefly, FT-IR spectroscopy in both transmission and attenuated total reflection (ATR) modes was used to study the overall averaged structure and surface layer of a Nafion 115 membrane. Nafion 115 is chemically identical to membranes used in our experiments (Nafion 117 and Nafion 212) but has a different membrane thickness of 125 μm. Comparison of transmission and ATR spectra showed a higher concentration of $–CF_2–$ in the overall averaged membrane than present just on the surface. As ATR spectroscopy penetrates several microns below the sample surface, these data also support the existence of a chemically distinct surface layer with a thickness of several microns. Additionally, both these previous FT-IR studies and our XPS data show a higher concentration of perfluoroethers buried within the inner bulk membrane, as the $–CF_2–$ groups of the main PTFE chain are co-localized next to the ether groups.

To further explore these discrete heterogeneous layers within Nafion membranes, sputter depth-profiling was performed on membrane surfaces via bombardment with argon ions. As the ions ablate the sample surface, changes in chemical composition can be measured in real time. Figure 6 shows C1s and O1s spectra collected at different time points during the sputtering process; a summary of atomic composition for each sputter interval is presented in Table II. The initial spectra collected prior to any sputtering measures the chemistry on the outermost surface of the membrane (black traces). Again, we observe distinct chemical differences between this layer and those tucked away deeper within the bulk material of the membrane. In the C1s spectra (Figure 6a), the signal from adventitious carbon disappears as sputtering progresses; a shoulder at ∼ 293.3 eV becomes visible, which corresponds to the $–CF_3$ groups of the side chain. Overall, we observe an increase in the percent composition of carbon from 39.2% before sputtering to 45.3% after 5 min of ablation. In the oxygen spectra (Figure 6b), the signals corresponding to the ether and sulfonate configurations are both present at the surface in nearly even ratios. After 30 seconds of sputtering (red trace), however, there is no longer evidence of sulfonate oxygen atoms. As the ablation of the membrane continues, the overall oxygen concentration decreases from 5.0% to 2.1% after 5 min. These sputtering profiles agree with the 2D mapping data presented above to highlight layered micro-heterogeneity: a

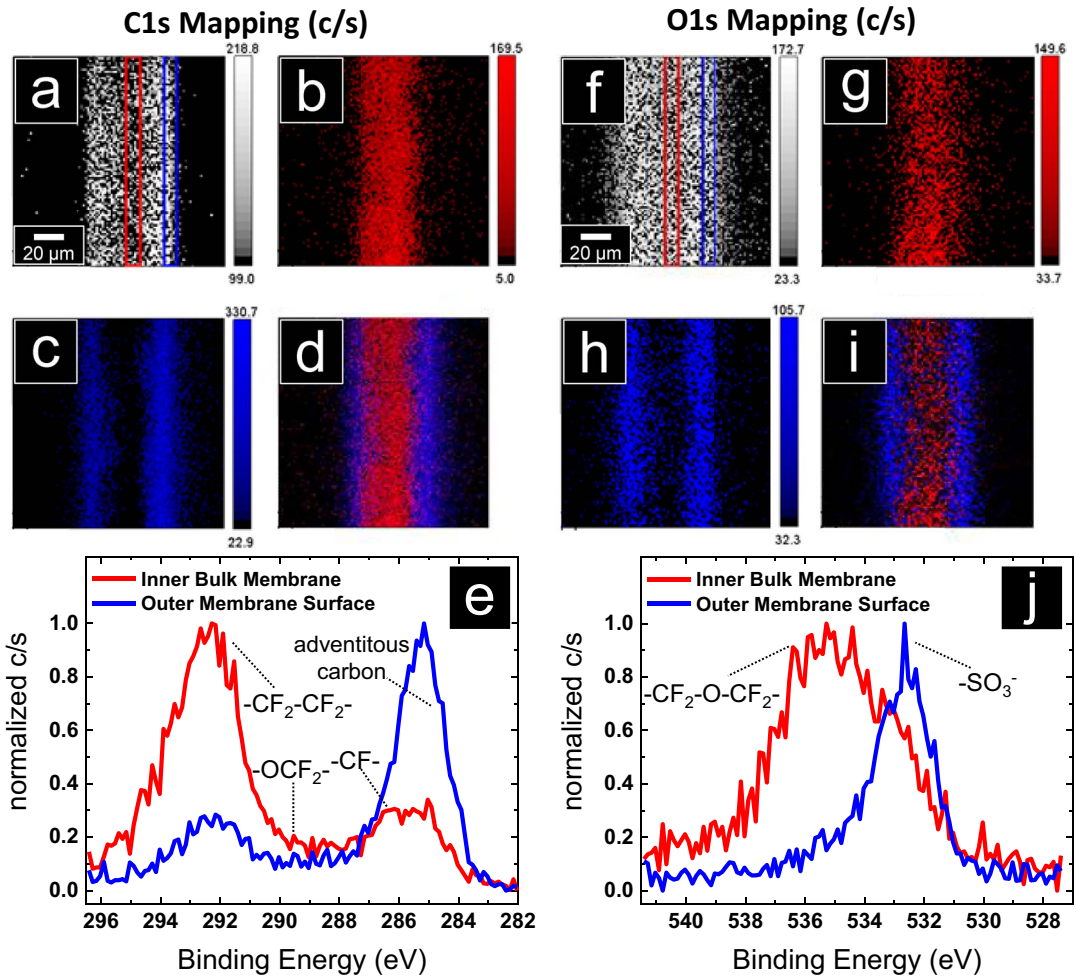

Figure 5. Two-dimensional XPS maps show discrete surface and bulk chemistry in Nafion membranes. The overall C1s elemental map of the cross section of an "As Purchased" 212 Nafion membrane is shown in (a). Within this map, the spectra of the inner bulk membrane (red box) and outer surface layer (blue box) were extracted and mapped in (b) and (c), respectively. An overlay of these two data sets is shown in (d). The spectra used to create these C1s maps are shown in (e); spectra have been normalized for easier visualization of compositional differences. Similarly, an overall O1s elemental map is presented in (f). Spectra of the inner bulk membrane (red box) and outer membrane surface (blue box) were mapped again in (g) and (h), respectively, with the overlay of these maps presented in (i). The corresponding extracted O1s spectra are displayed in (j), with the counts normalized for easier comparison.

surface layer rich in polar sulfonate groups shields an inner hydrophobic bulk material. Non-destructive sputter depth-profiling with a gas cluster ion beam (GCBI, Ar_{2500}^{+}) was also performed and in good agreement with the above data (SI Figure S9).

Conclusions

With the use of HOPG as an internal standard and calibrant for XPS analysis, proper binding energy peaks for C1s, O1s, F1s and S2p spectra in Nafion membranes have been carefully assigned in an attempt to solve a long-standing discrepancy in oxygen configuration assignment. The higher binding energy signal (~535.5 eV) corresponds to oxygen in the ether configuration due to a fluorine-rich, electronegative environment; the lower binding energy signal (~533.1 eV) originates from the sulfonate head group. Additionally, a heterogeneous microstructure within these membranes was demonstrated from two-dimensional XPS elemental mapping and sputter depth-profiling. Discrete surface layers and inner bulk material were shown to have vastly different chemical compositions, with polar sulfonate groups positioned on the outer surface. The higher surface free energy of sulfonate functional groups in comparison to the fluorinated backbone likely drives this observed segregation. Understanding the microarchitecture of Nafion will likely prove important to prevent membrane degradation that presently plagues fuel cells. Studies reported here are focused on commercially prepared Nafion films, but the exact origins of the phase separation are not explicitly investigated. The microscale segregation observed could be augmented by different casting or thermal treatments during preparation and if thicker films are used, microscale domain formation is worth considering for more diverse applications such as chemically

Table II. Elemental composition (in atomic percentage) of Nafion membranes after different sputtering exposure times as determined from XPS spectra shown in Fig. 6.

Sample	C1s (%)	O1s (%)	F1s (%)	S2p (%)
Expected Values from Chemical Formula	30.8	7.7	60.0	1.5
Initial Membrane	*39.2*[a]	*5.0*	*55.3*	*0.5*
Sputtered 30 sec	*42.0*	*3.4*	*54.2*	*0.4*
Sputtered 1 min	*44.7*	*2.9*	*52.0*	*0.4*
Sputtered 5 min	*45.3*	*2.1*	*52.4*	*0.2*

[a]Italicized entries are experimental results.

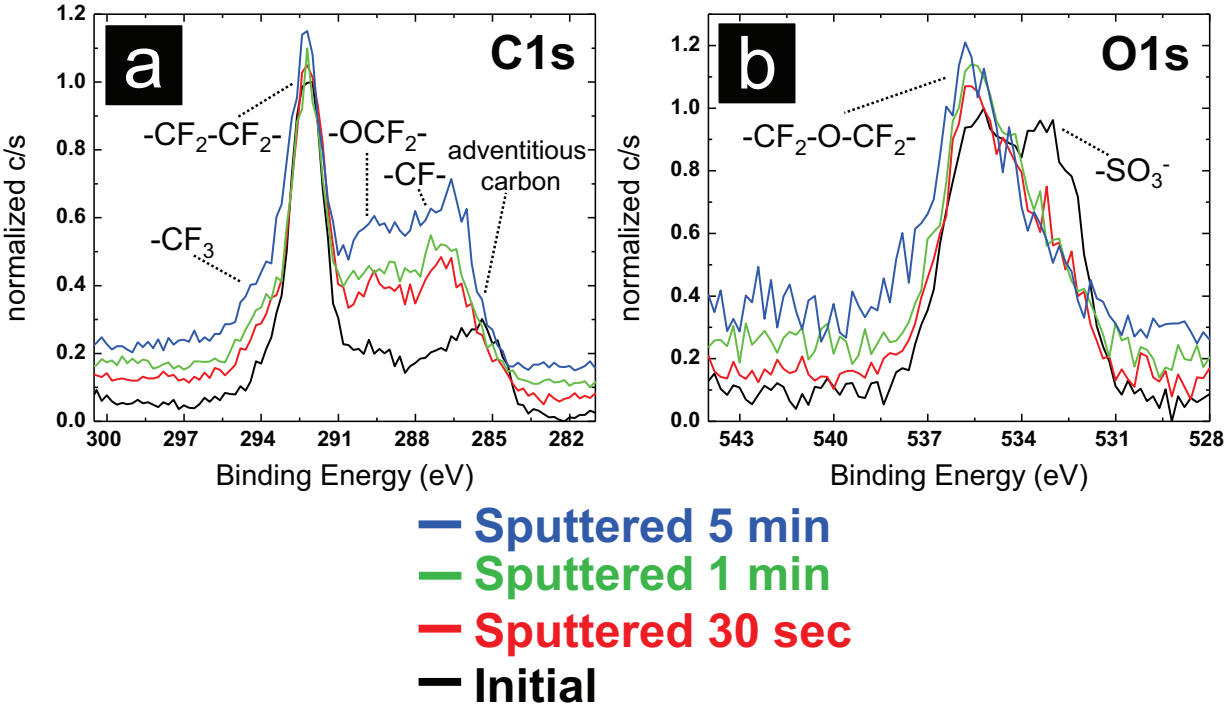

Figure 6. Normalized C1s (a) and O1s (b) spectra of "As Purchased" Nafion membranes after different exposure times to Ar^+ sputtering (2 keV): initial pre-sputtering surface (black), 30 s exposure (red), 1 min exposure (green) and 5 min exposure (blue). Traces have been offset for easier visualization.

modified electrodes or biosensors as well. Future work in this area may include studies of the effects of microstructure on chemical transport, membrane-arrangement kinetics after exposure of inner bulk material, and optimization of surface layer modifications for better sensing platforms.

Acknowledgments

Support from the National Science Foundation (CMI Award 1507341) is gratefully acknowledged. Access to XPS at the Nanoscale Characterization Facility was provided by the NSF Award DMR MRI-1126394. Non-destructive sputter depth-profiling with argon clusters (GCIB) was graciously performed by Physical Electronics. SEM analysis was accomplished thanks to support from the Nanoscale Characterization Facility. Financial support provided by Indiana University is gratefully acknowledged. The authors thank Dr. Dmitri Petrovykh (International Iberian Nanotechnology Laboratory) for insightful scientific discussions.

ORCID

Lane A. Baker https://orcid.org/0000-0001-5127-507X

References

1. H. W. Zhang and P. K. Shen, *Chem. Rev.*, **112**, 2780 (2012).
2. K. A. Mauritz and R. B. Moore, *Chem. Rev.*, **104**, 4535 (2004).
3. M. Yoshitake and A. Watakabe, *Adv. Polym. Sci.*, **215**, 127 (2008).
4. Y. Nagao, *Langmuir*, **33**, 12547 (2017).
5. A. Kusoglu and A. Z. Weber, *Chem. Rev.*, **117**, 987 (2017).
6. K. Schmidt-Rohr and Q. Chen, *Nat. Mater.*, **7**, 75 (2008).
7. K. D. Kreuer and G. Portale, *Adv. Funct. Mater.*, **23**, 5390 (2013).
8. N. J. C. Ingle, A. Sode, I. Martens, E. Gyenge, D. P. Wilkinson, and D. Bizzotto, *Langmuir*, **30**, 1871 (2014).
9. W. Grot, *Fluorinated Ionomers*, C. G. Processing, Inc., Chadds Ford, PA (2011).
10. E. A. Ticianelli, C. R. Derouin, and S. Srinivasan, *J. Electroanal. Chem.*, **251**, 275 (1988).
11. F. M. Pan, Y. L. Lin, and S. R. Horng, *Appl. Surf. Sci.*, **47**, 9 (1991).
12. T. A. Zawodzinski, C. Derouin, S. Radzinski, R. J. Sherman, V. T. Smith, T. E. Springer, and S. Gottesfeld, *J. Electrochem. Soc.*, **140**, 1041 (1993).
13. G. Schwitzgebel and F. Endres, *J. Electroanal. Chem.*, **386**, 11 (1995).
14. W. M. Grava, T. Okada, and Y. Kawano, *Electrochemistry*, **74**, 467 (2006).
15. M. Schulze, M. Lorenz, N. Wagner, and E. Gulzow, *Fresen. J. Anal. Chem.*, **365**, 106 (1999).
16. T. Kinumoto, M. Inaba, Y. Nakayama, K. Ogata, R. Umebayashi, A. Tasaka, Y. Iriyama, T. Abe, and Z. Ogumi, *J. Power Sources*, **158**, 1222 (2006).
17. R. C. T. Slade, J. Barker, and J. H. Strange, *Solid State Ionics*, **35**, 11 (1989).
18. W. Shi and L. A. Baker, *RSC Adv.*, **5**, 99284 (2015).
19. G. Rambabu, N. Nagaraju, and S. D. Bhat, *Chem. Eng. J.*, **306**, 43 (2016).
20. W. Jia, B. B. Tang, and P. Y. Wu, *ACS Appl. Mater. Interfaces*, **9**, 14791 (2017).
21. A. Donnadio, R. Narducci, M. Casciola, F. Marmottini, R. D'Amato, M. Jazestani, H. Chiniforoshan, and F. Costantino, *ACS Appl. Mater. Interfaces*, **9**, 42239 (2017).
22. K. S. Novoselov, A. K. Geim, S. V. Morozov, D. Jiang, Y. Zhang, S. V. Dubonos, I. V. Grigorieva, and A. A. Firsov, *Science*, **306**, 666 (2004).
23. E. A. Hoffmann, Z. A. Fekete, L. S. Korugic-Karasz, F. E. Karasz, and E. Wilusz, *J. Polym. Sci. Pol. Chem.*, **42**, 551 (2004).
24. S. J. Schmieg and D. N. Belton, *Surf. Sci. Spectra*, **1**, 333 (1992).
25. D. T. Clark, W. J. Feast, D. Kilcast, and W. K. Musgrave, *J. Polym. Sci. Pol. Chem.*, **11**, 389 (1973).
26. G. Beamson and D. Briggs, *High Resolution XPS of Organic Polymers: The Scienta ESCA300 Database*, p. 295, Wiley, Chichester [England]; New York (1992).
27. M. Toselli, J. A. Gardella, M. Messori, A. M. Hawkridge, F. Pilati, and C. Tonelli, *Polym. Int.*, **52**, 1262 (2003).
28. M. M. Nasef, H. Saidi, H. M. Nor, and M. A. Yarmo, *J. Appl. Polym. Sci.*, **76**, 336 (2000).
29. M. K. Younes, A. Ghorbel, A. Rives, and R. Hubaut, *J. Sol-Gel Sci. Techn.*, **19**, 817 (2000).
30. J. Huslage, T. Rager, B. Schnyder, and A. Tsukada, *Electrochim. Acta*, **48**, 247 (2002).
31. C. Y. Yen, C. H. Lee, Y. F. Lin, H. L. Lin, Y. H. Hsiao, S. H. Liao, C. Y. Chuang, and C. C. M. Ma, *J. Power Sources*, **173**, 36 (2007).
32. X. G. Ding, S. M. Zhou, L. F. Jiang, and H. Yang, *J. Sol-Gel Sci. Techn.*, **58**, 345 (2011).
33. M. Vijayakumar, M. S. Bhuvaneswari, P. Nachimuthu, B. Schwenzer, S. Kim, Z. G. Yang, J. Liu, G. L. Graff, S. Thevuthasan, and J. Z. Hu, *J. Membrane Sci.*, **366**, 325 (2011).
34. M. V. M. de Yuso, L. A. Neves, I. M. Coelhoso, J. G. Crespo, J. Benavente, and E. Rodriguez-Castellon, *Fuel Cells*, **12**, 606 (2012).
35. A. Khot, F. Lu, T. Debies, and G. A. Takacs, *J. Adhes. Sci. Technol.*, **27**, 309 (2013).
36. M. D. M. de Yuso, M. T. Cuberes, V. Romero, L. Neves, I. Coelhoso, J. G. Crespo, E. Rodriguez-Castellon, and J. Benauente, *Int. J. Hydrogen Energ.*, **39**, 4023 (2014).
37. S. M. Andersen, R. Dhiman, and E. Skou, *J. Power Sources*, **282**, 87 (2015).
38. M. V. M. de Yuso, A. B. Calderon, V. Romero, M. T. Cuberes, and J. Benavente, *Surf. Interface Anal.*, **48**, 561 (2016).

39. W. White, C. D. Sanborn, R. S. Reiter, D. M. Fabian, and S. Ardo, *J. Am. Chem. Soc.*, **139**, 11726 (2017).
40. M. D. M. de Yuso, A. Arango-Diaz, S. Bijani, V. Romero, J. Benavente, and E. Rodriguez-Castellon, *Appl. Sci.*, **4**, 195 (2014).
41. I. G. Casella, *J. Appl. Electrochem.*, **31**, 481 (2001).
42. C. Chen, G. Levitin, D. W. Hess, and T. F. Fuller, *J. Power Sources*, **169**, 288 (2007).
43. Z. B. Wang, P. J. Zuo, Y. Y. Chu, Y. Y. Shao, and G. P. Yin, *Int. J. Hydrogen Energ.*, **34**, 4387 (2009).
44. C. Chen and T. F. Fuller, *J. Electrochem. Soc.*, **156**, B1218 (2009).
45. V. Parry, G. Berthome, J. C. Joud, O. Lemaire, and A. A. Franco, *J. Power Sources*, **196**, 2530 (2011).
46. M. Vijayakumar, B. Schwenzer, S. Kim, Z. G. Yang, S. Thevuthasan, J. Liu, G. L. Graff, and J. Z. Hu, *Solid State Nucl. Mag.*, **42**, 71 (2012).
47. Y. Zhu, S. P. Pei, J. K. Tang, H. Li, L. Wang, W. Z. Yuan, and Y. M. Zhang, *J. Membrane Sci.*, **432**, 66 (2013).
48. S. J. Lue, Y. L. Pai, C. M. Shih, M. C. Wu, and S. M. Lai, *J. Membrane Sci.*, **493**, 212 (2015).
49. W. M. Qiu, R. Muller, E. Voroshazi, B. Conings, R. Carleer, H. G. Boyen, M. Turbiez, L. Froyen, P. Heremans, and A. Hadipour, *ACS Appl. Mater. Inter.*, **7**, 3581 (2015).
50. L. W. Yu, Y. Takagi, T. Nakamura, O. Sekizawa, T. Sakata, T. Uruga, M. Tada, Y. Iwasawa, G. Samjeske, and T. Yokoyama, *Phys. Chem. Chem. Phys.*, **19**, 30798 (2017).
51. M. Schulze, M. von Bradke, R. Reissner, M. Lorenz, and E. Gulzow, *Fresen. J. Anal. Chem.*, **365**, 123 (1999).
52. J. F. Moulder, W. F. Stickle, P. E. Sobol, and K. D. Bomben, *Handbook of X-ray Photoelectron Spectroscopy: A Reference Book of Standard Spectra for Identification and Interpretation of XPS Data*, Physical Electronics Division, Perkin-Elemer Corp.: Eden Prarie, Minn. (1992).
53. F. A. Bottino, G. Di Pasquale, A. Pollicino, F. Pilati, M. Toselli, and C. Tonelli, *Macromolecules*, **31**, 7814 (1998).
54. G. P. Lopez, D. G. Castner, and B. D. Ratner, *Surf. Interface Anal.*, **17**, 267 (1991).
55. Z. X. Liang, W. M. Chen, J. G. Liu, S. L. Wang, Z. H. Zhou, W. Z. Li, G. Q. Sun, and Q. Xin, *J. Membrane Sci.*, **233**, 39 (2004).